

Dinuclear silver(I) nitrate complexes with bridging bisphosphinomethanes: argentophilicity and luminescence

Kristina F. Baranova^{1,2}, Aleksei A. Titov^{*1}, Oleg A. Filippov^{1,3} Alexander F. Smol'yakov¹, Alexey A. Averin⁴, Elena S. Shubina^{*1}

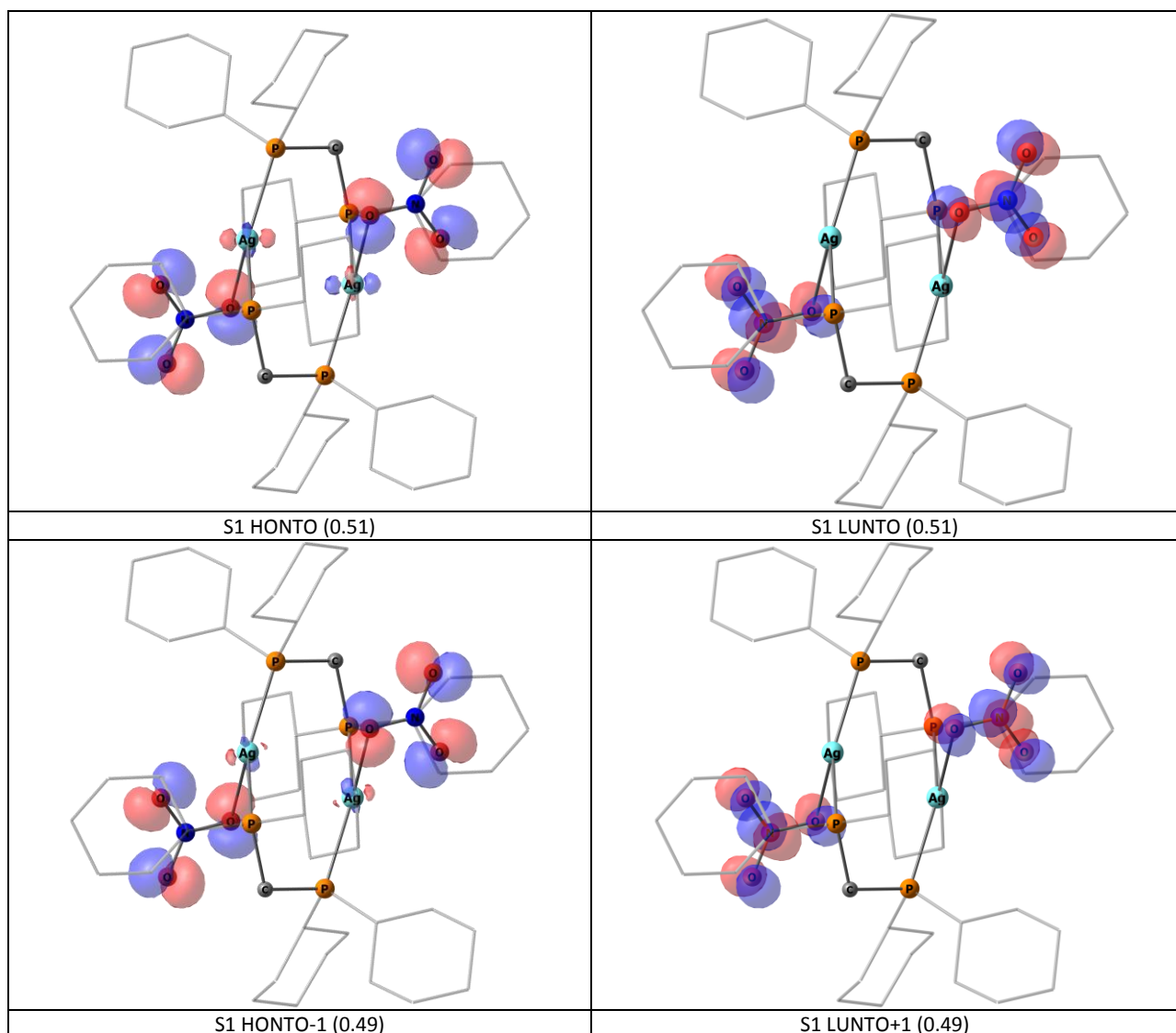
¹ A. N. Nesmeyanov Institute of Organoelement Compounds, Russian Academy of Sciences, Vavilov Str., 28, 119991, Moscow, Russia. E-mail: krisbar99@gmail.com, tit@ineos.ac.ru, h-bond@ineos.ac.ru, rengenhik@gmail.com, shu@ineos.ac.ru.

² Lomonosov Moscow State University, Faculty of Chemistry, 1-3 Leninskie Gory, 119991, Moscow, Russia.

³ Shemyakin-Ovchinnikov Institute of Bioorganic Chemistry, Russian Academy of Sciences, Miklukho-Maklaya st., 16/10, 117997, Moscow, Russia.

⁴ A. N. Frumkin Institute of Physical Chemistry and Electrochemistry, Leninsky pros. 31/4, 119071 Moscow, Russian Academy of Sciences, 199071 Moscow, Russia. E-mail: alx.av@yandex.ru.

* Correspondence: shu@ineos.ac.ru, tit@ineos.ac.ru; Tel.: +7-495-135-5085



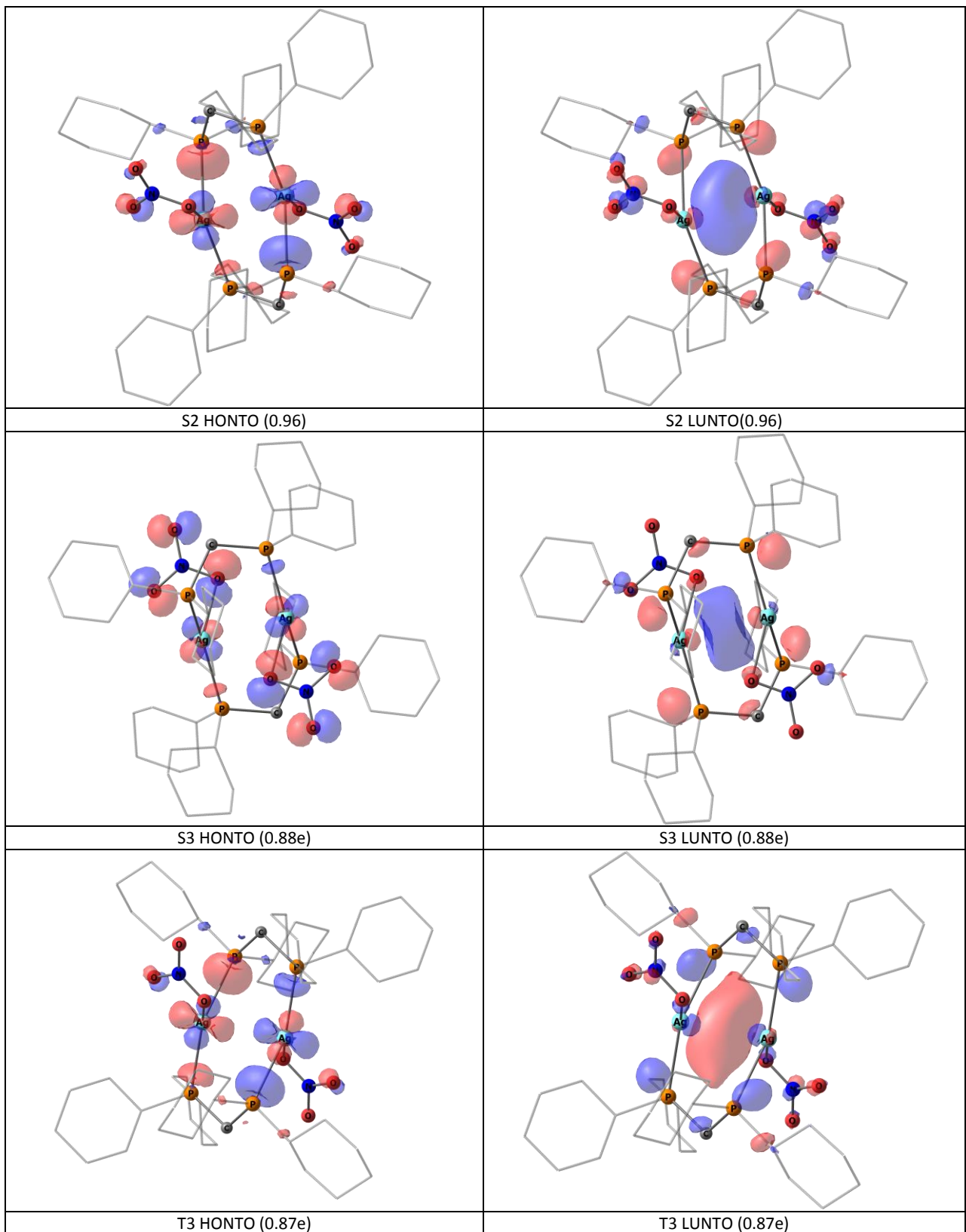
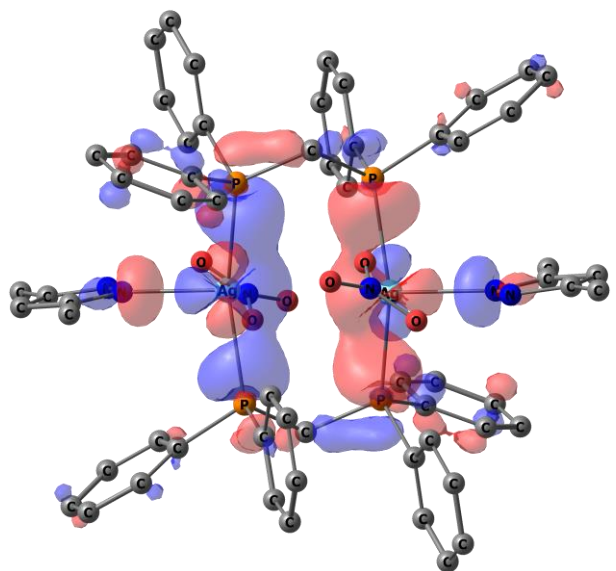


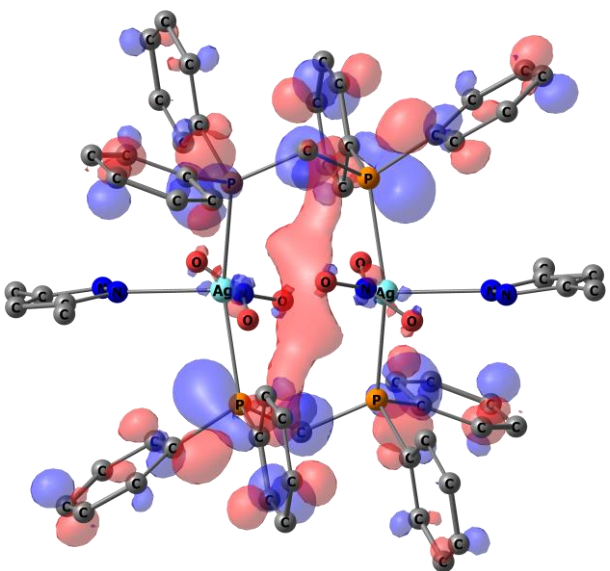
Figure S1. Natural transition orbitals of **1** as isosurface at 0.05 a.u.

Table S1. Computed characteristics of the excited states of **1**. For analysis of fragment impacts (in %) to the ground state (hole) and excited state (electron) complex was divided to fragments of all Ag atoms, all P atoms, nitrate anions and all atoms of dcypm ligand except P.

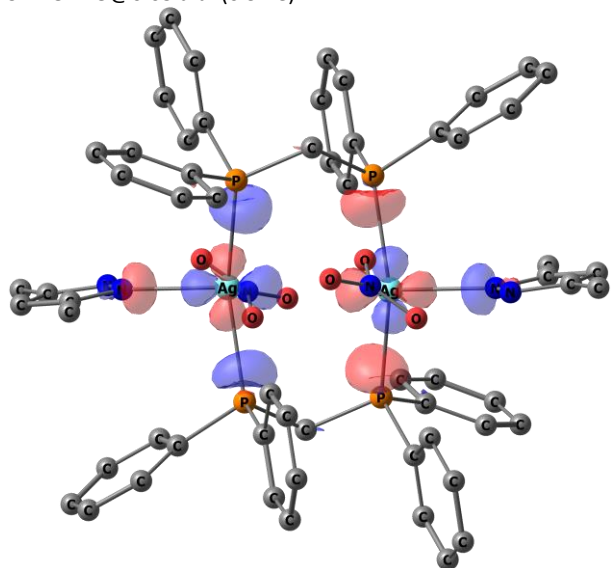
#	E, eV	f	Composition of hole				Composition of electron			
			Ag	P	NO ₃	dcypm	Ag	P	NO ₃	dcypm
S1	4.1806	0.0002	3.3	0.2	95.7	0.8	1.8	1.5	93.1	3.6
S2	5.0148	0.1853	40.4	35.6	9.1	14.8	29.8	36.6	15.2	18.4
S3	5.3326	0.0422	16.3	11.2	66.9	5.6	30.3	37.2	11.7	20.8
S4	5.3609	0.0294	35.3	33.0	18.1	13.5	6.7	9.2	72.9	11.2
S5	5.4226	0.0311	24.1	40.0	16.9	19.0	31.0	37.2	11.8	19.9
S6	5.6751	0.0394	31.9	39.3	12.8	16.0	3.9	5.9	81.7	8.5
T1	3.7074	-	2.1	0.1	97.0	0.8	1.2	0.9	95.5	2.4
T2	4.3058	-	3.4	5.0	89.5	2.2	2.0	1.5	94.3	2.2
T3	4.5959	-	37.9	37.1	11.4	13.6	30.8	38.7	12.5	18.1
T4	4.7181	-	5.4	4.0	88.5	2.1	2.6	2.7	90.8	3.9
T5	4.9614	-	23.4	52.1	3.8	20.7	29.1	46.3	3.8	20.8
T6	5.2128	-	28.8	24.8	36.0	10.5	9.5	12.7	66.4	11.5



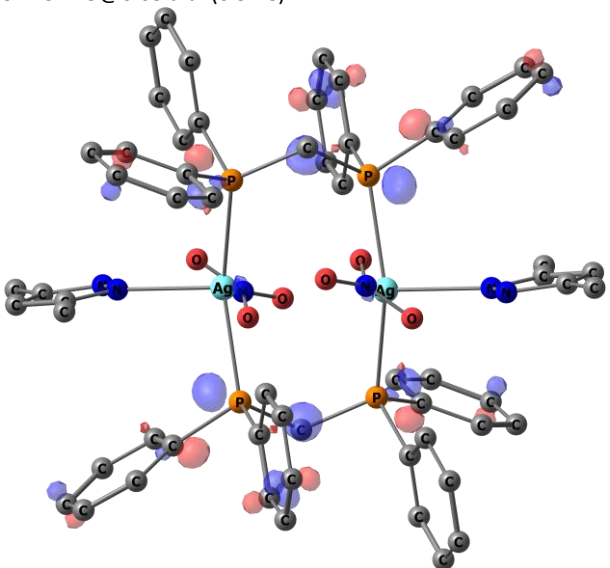
S1 HONTO@0.03 a.u. (0.97 e)



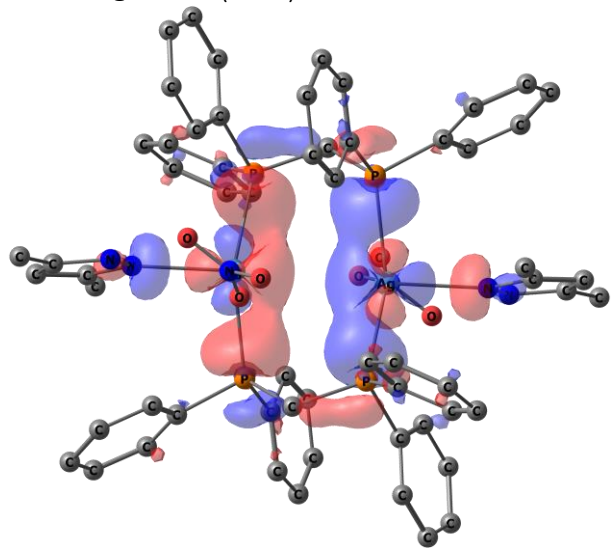
S1 LUNTO@0.03 a.u. (0.97 e)



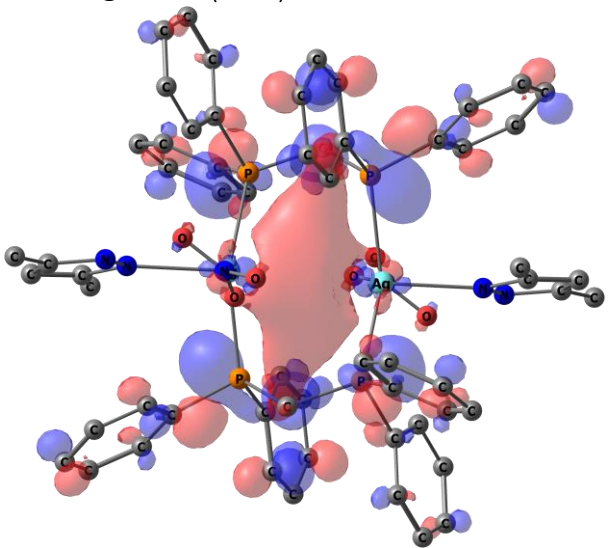
S1 HONTO@0.05 a.u. (0.97 e)



S1 LUNTO@0.05 a.u. (0.97 e)



T6 HONTO@0.03 a.u. (0.75 e)



T6 LUNTO@0.03 a.u. (0.75 e)

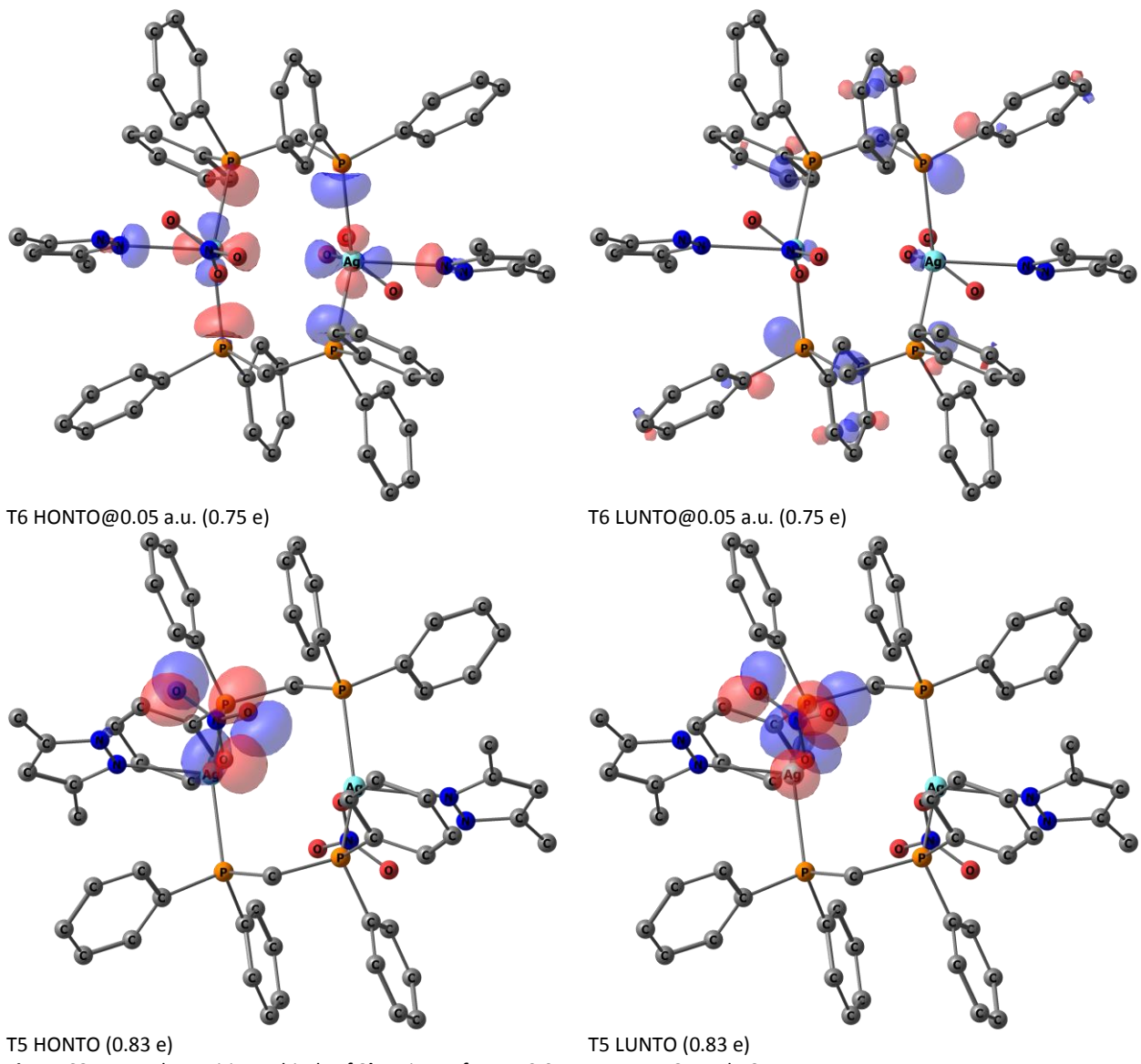
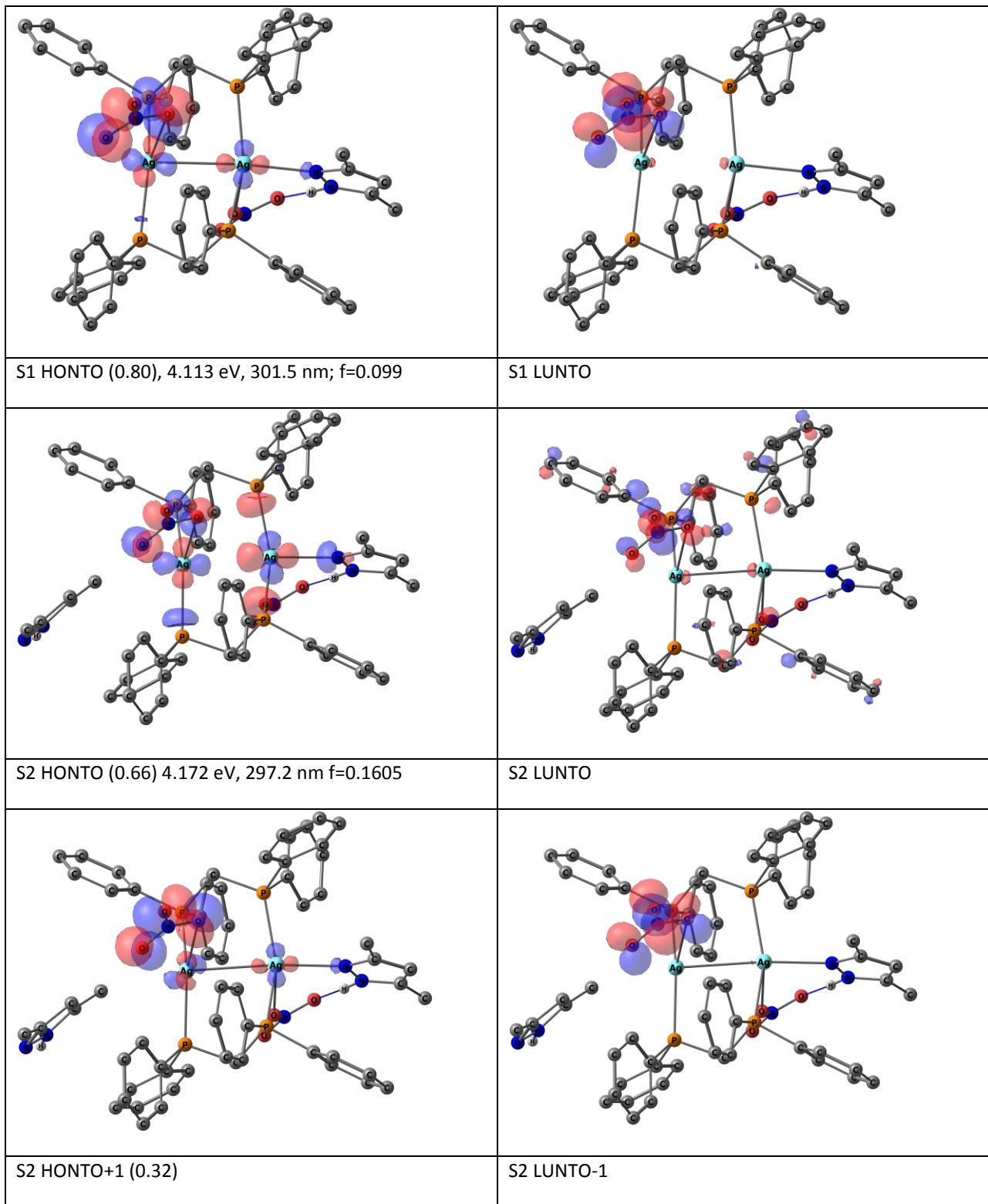


Figure S2. Natural transition orbitals of **2b** as isosurface at 0.05 a.u. except S1 and T6

Table S2. Computed characteristics of the Au symmetry excited states of 2a. For analysis of fragment impacts (in %) to the ground state (hole) and excited state (electron) complex was divided to fragments of all Ag atoms, all P atoms, nitrate anions, pyrazolates and all atoms of dppm ligand except P.

#	E, eV	f	Composition of hole					Composition of electron				
			Ag	P	NO ₃	Pz	dppm	Ag	P	NO ₃	Pz	dppm
S1	4.1569	0.2354	35.1	32.8	0.4	9.6	22.1	9.9	24.2	2.0	0.4	63.5
S2	4.2291	0.0009	1.9	0.5	96.5	0.7	0.4	3.1	1.2	89.2	1.0	5.7
S3	4.4430	0.0243	31.2	33.0	0.5	9.2	26.1	2.6	8.5	1.8	0.2	86.9
S4	4.5290	0.0329	30.4	33.9	1.0	8.7	26.0	4.1	9.7	1.8	0.2	84.2
S5	4.6459	0.1230	20.4	33.5	2.6	16.4	27.1	8.4	20.9	1.6	0.4	68.8
S6	4.8274	0.0509	18.1	33.1	4.5	12.9	31.3	0.6	13.3	0.2	0.2	85.8
T1	3.3834	-	5.6	10.2	0.0	0.4	83.9	3.1	8.0	0.7	0.3	87.8
T2	3.4336		2.8	7.1	0.0	0.2	90.1	1.4	5.4	0.0	0.5	92.9
T3	3.4874	-	0.0	0.6	0.1	0.0	99.5	0.1	3.2	0.0	0.1	96.7
T4	3.5037		0.0	0.5	0.1	0.0	99.5	0.2	3.2	0.0	0.1	96.5
T5	3.7643	-	1.4	0.3	97.4	0.5	0.5	2.0	0.5	93.8	0.9	2.9
T6	4.0184		32.6	31.1	0.7	9.0	26.6	11.9	26.0	1.6	0.6	60.0



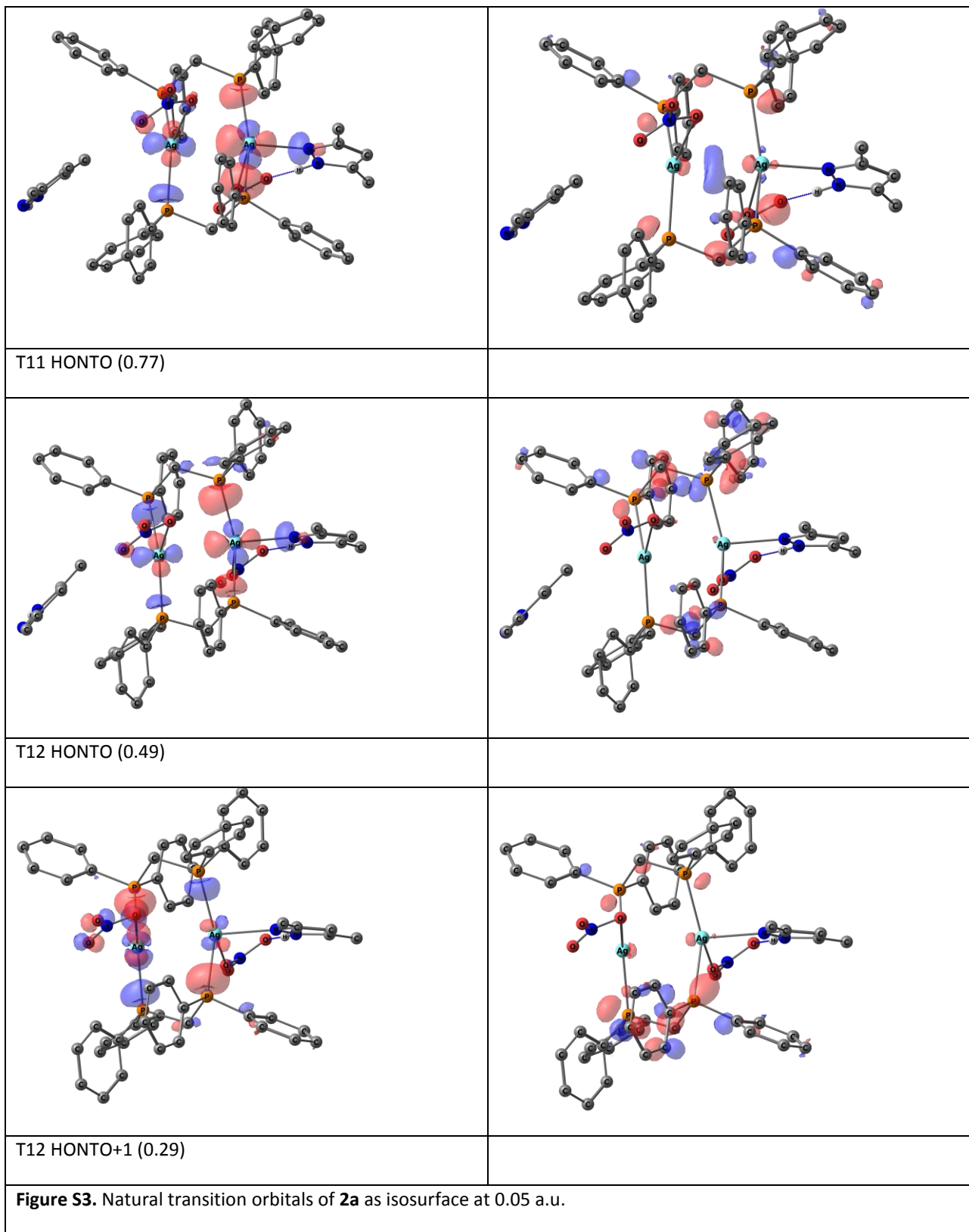


Table S3. Computed characteristics of the A_u symmetry excited states of **2a**. For analysis of fragment impacts (in %) to the ground state (hole) and excited state (electron) complex was divided to fragments of all Ag atoms, all P atoms, nitrate anions, pyrazolates and all atoms of dppm ligand except P.

#	E, eV	f	Composition of hole					Composition of electron				
			Ag	P	NO_3	Pz	dppm	Ag	P	NO_3	Pz	dppm
S1	4.1127	0.0990	17.5	12.9	58.5	2.2	8.9	8.2	11.1	52.3	0.7	27.7
S2	4.1716	0.1605	24.8	21.4	34.5	3.9	15.3	8.4	16.6	33.3	0.7	41.0
S3	4.2363	0.0005	2.1	0.4	95.4	1.6	0.6	3.8	1.8	87.5	0.7	6.2
S4	4.3506	0.0000	28.7	32.5	7.5	5.8	25.5	2.3	18.8	-0.1	0.3	78.6
S5	4.4559	0.0365	14.6	19.5	30.8	21.3	13.9	10.3	22.8	0.8	1.1	65.0
S6	4.4943	0.0074	4.5	5.9	7.8	73.7	8.2	10.4	21.9	1.3	1.1	65.2
T1	3.3890	-	6.2	11.1	0.1	0.3	82.4	4.3	9.3	0.3	0.7	85.4
T2	3.4077	-	4.0	9.4	-0.2	-0.1	86.9	2.6	7.0	0.5	0.4	89.6
T3	3.4436	-	2.6	6.6	-0.9	0.1	91.6	2.0	5.7	-0.3	0.7	91.8
T4	3.4640	-	1.9	5.6	0.2	-1.3	93.6	1.1	5.0	0.0	0.4	93.4
T5	3.4832	-	-0.4	0.4	-0.6	0.1	100.5	0.1	4.1	0.0	0.2	95.6
T6	3.4838	-	-0.1	0.3	-0.1	-0.6	100.5	-0.1	3.4	0.1	0.3	96.2
T7	3.5033	-	-0.3	0.2	0.0	-0.3	100.4	0.3	3.4	-0.2	0.2	96.4
T8	3.5053	-	-0.3	0.4	-0.6	-0.7	101.2	0.0	3.8	-0.1	0.3	95.9
T9	3.6726	-	5.2	0.7	94.2	-1.0	1.0	1.5	0.5	93.5	0.1	4.5
T10	3.7754	-	1.1	0.3	97.4	0.5	0.7	2.1	0.7	93.5	0.5	3.1
T11	3.9821	-	34.6	31.1	5.2	7.1	21.9	18.9	28.0	1.7	1.5	49.9
T12	4.2096	-	24.4	34.5	5.5	4.2	31.5	4.9	22.1	0.4	0.7	72.0

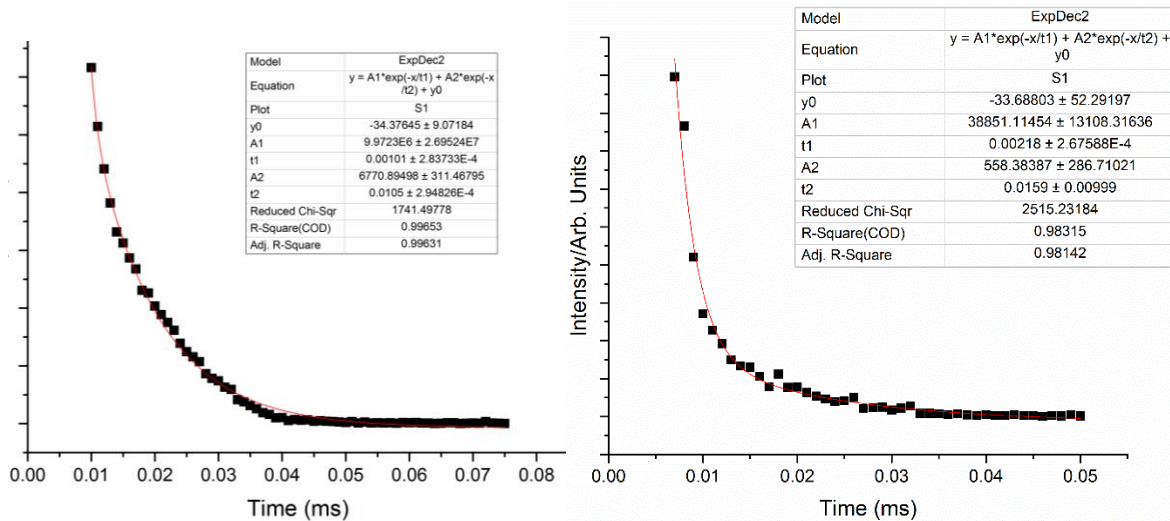


Figure S4. Phosphorescence decay by delay of complex **1** at RT in CH_2Cl_2 solution (left) and solid state (right).

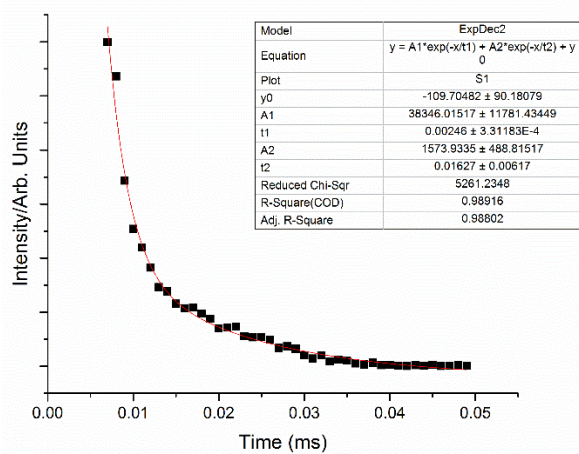


Figure S5. Phosphorescence decay by delay of complex **1** in the solid state at 77 K.

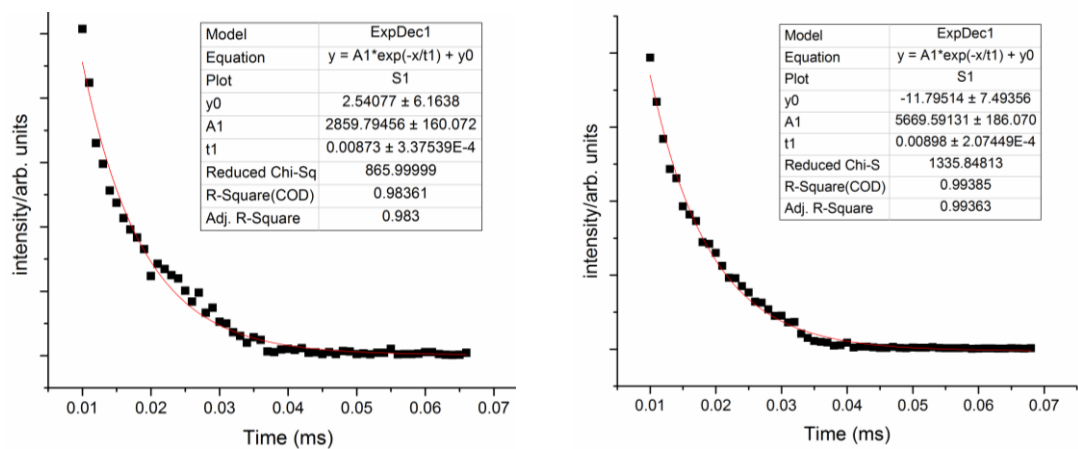


Figure S6. Phosphorescence decay by delay of complex **2a** at RT in CH_2Cl_2 solution (left) and solid state (right).

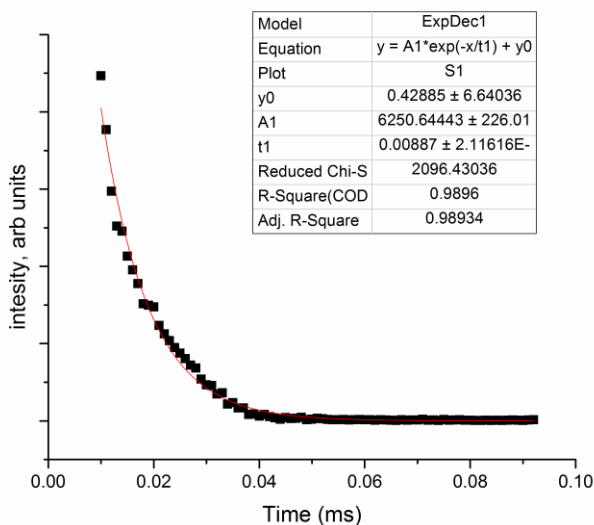


Figure S7. Phosphorescence decay by delay of complex **2a** in the solid state at 77 K (measured at 390 nm).

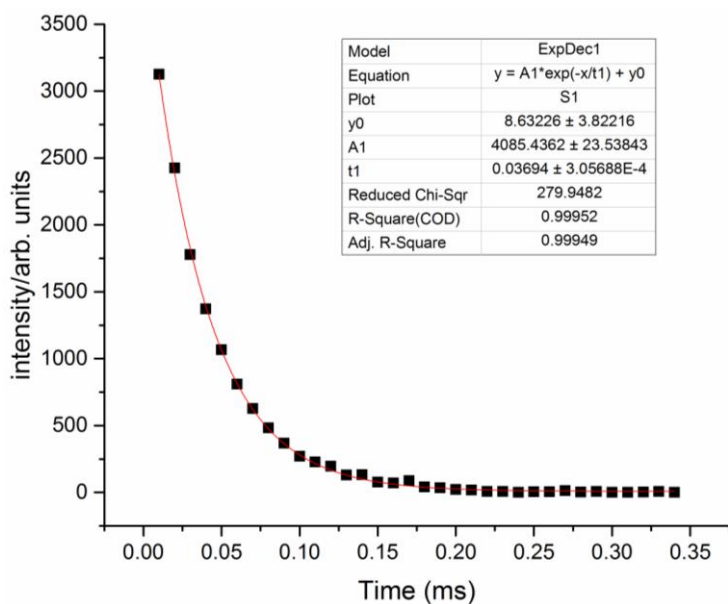


Figure S8. Phosphorescence decay by delay of complex **2a** in the solid state at 77 K (measured at 440 nm).

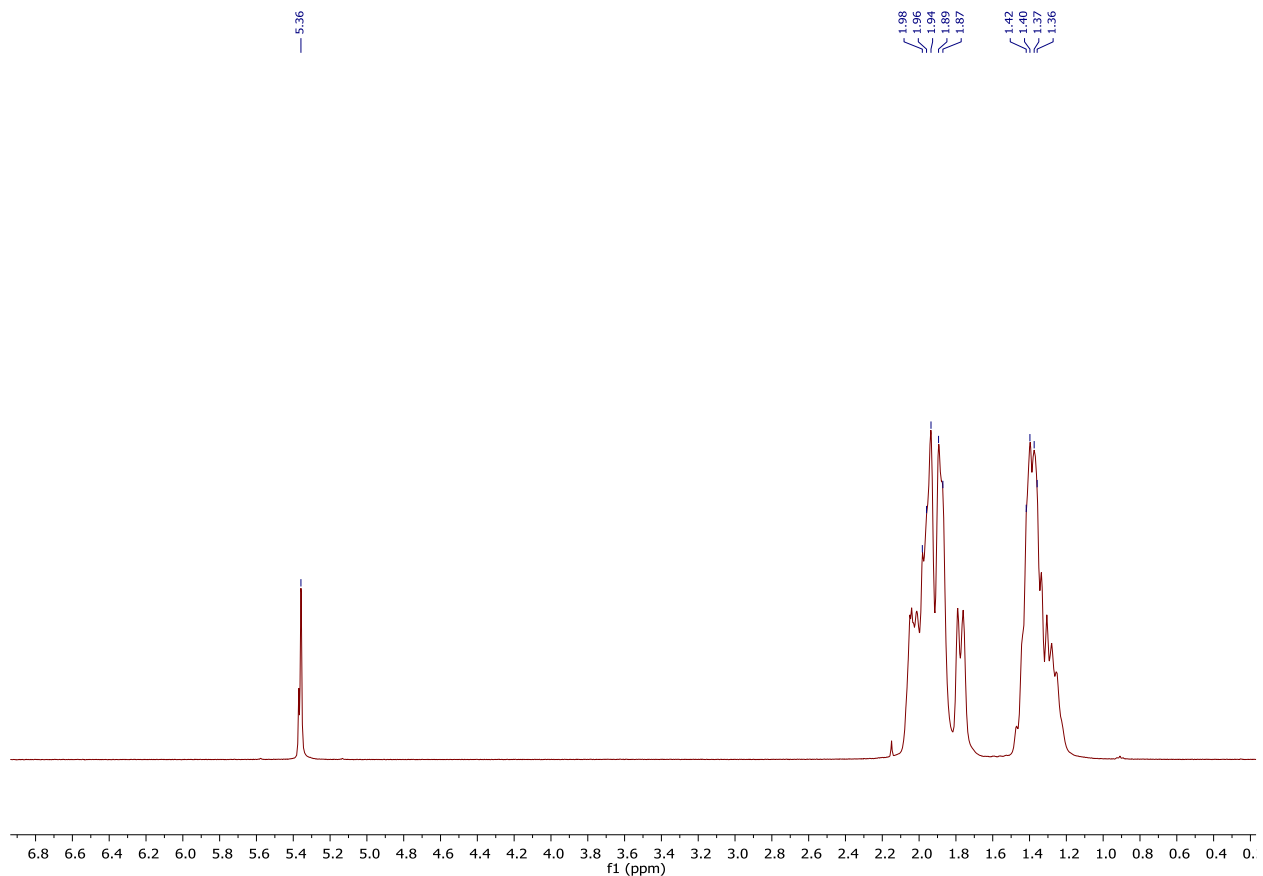


Figure S9. The ¹H NMR spectrum of complex **1** in CD_2Cl_2 .

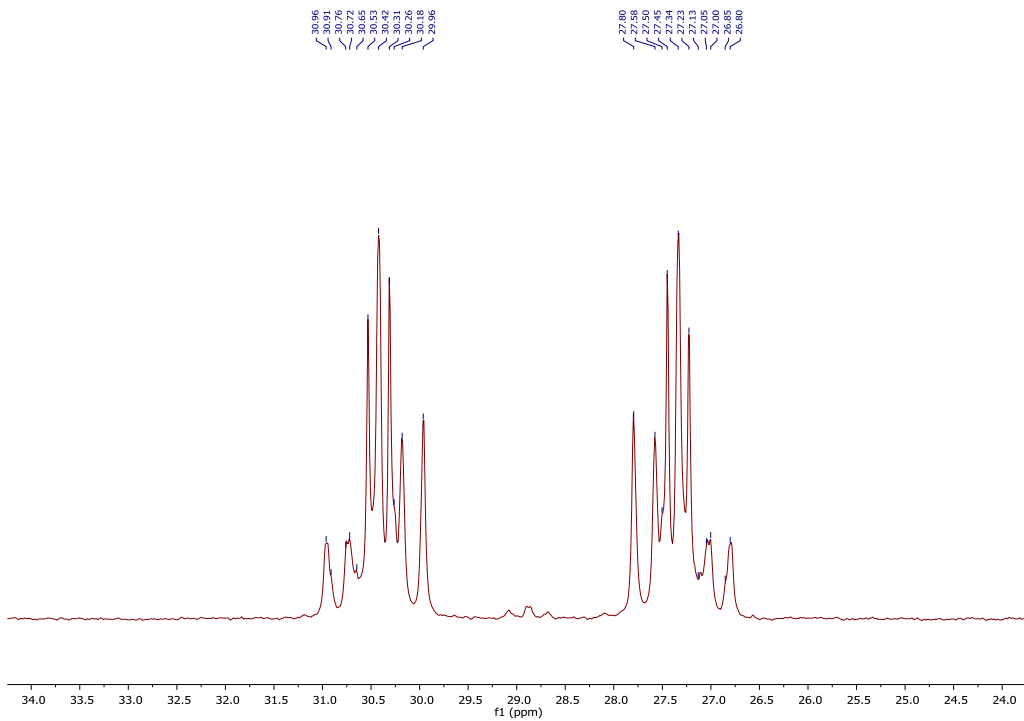


Figure S10. The $^{31}\text{P}\{\text{H}\}$ NMR spectrum of complex **1** in CD_2Cl_2 .

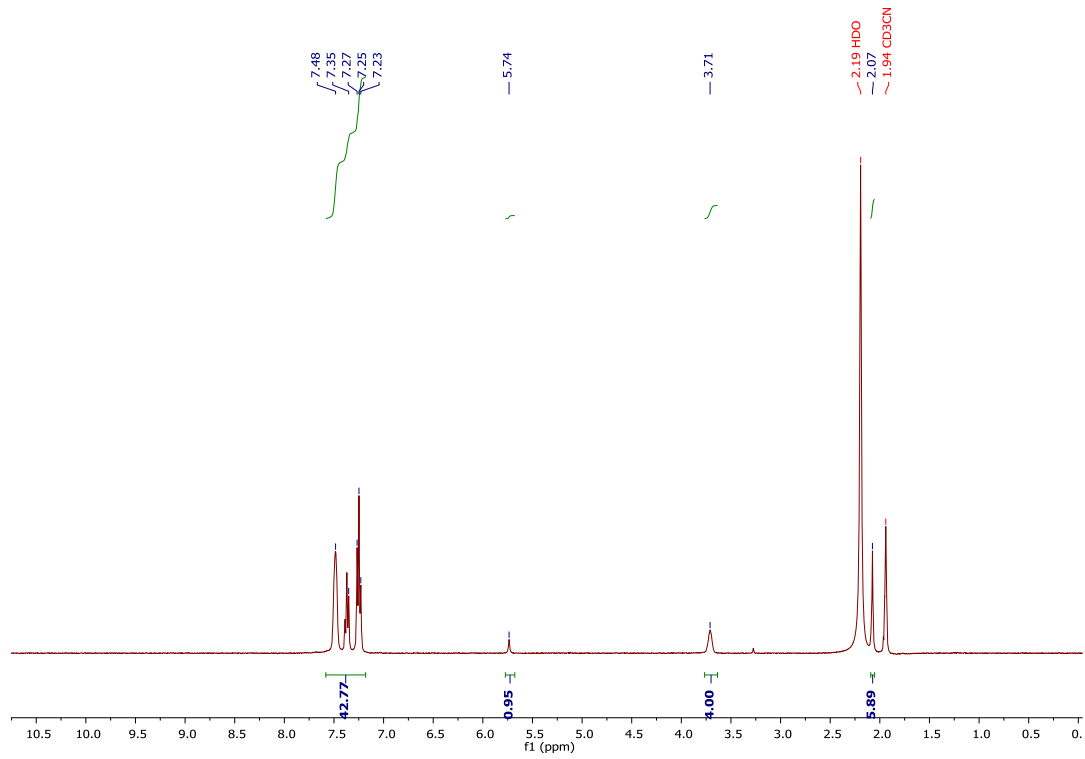


Figure S11. The ^1H NMR spectrum of complex **2a** in CD_3CN .

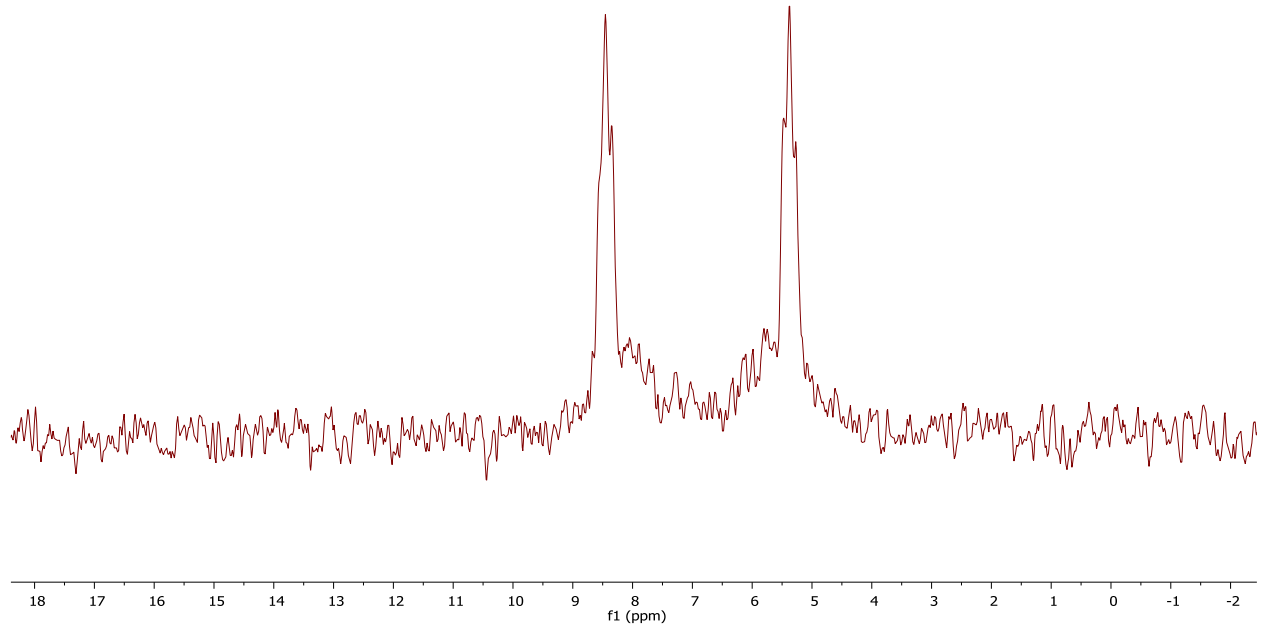


Figure S12. The $^{31}\text{P}\{\text{H}\}$ NMR spectrum of complex **2a** in CD_3CN .

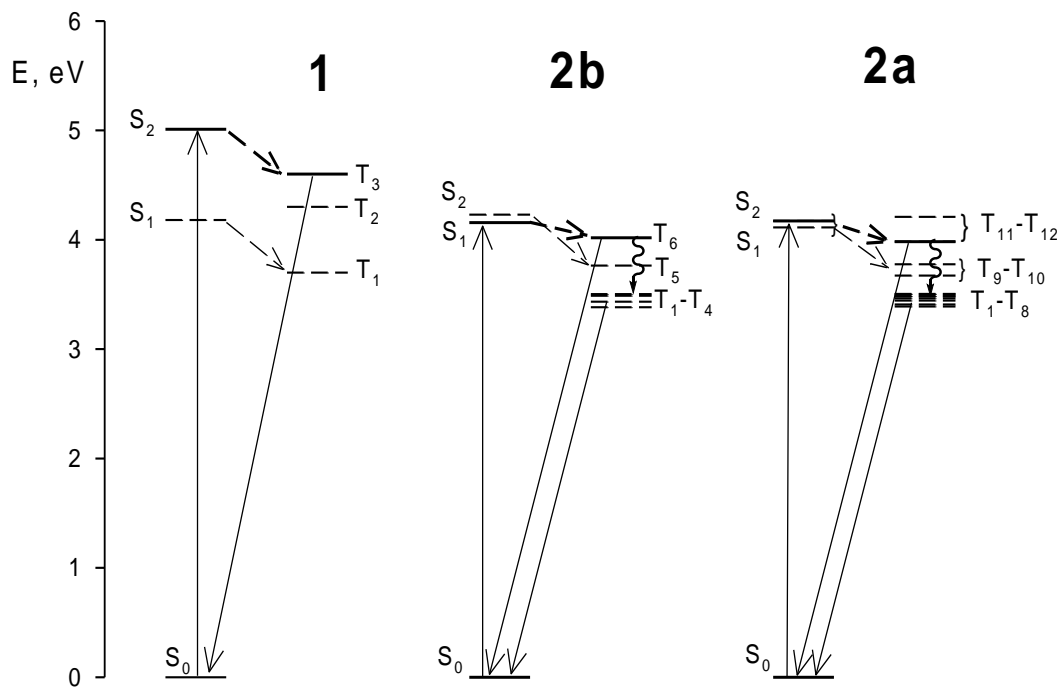


Figure S13. Schematic Jablonski diagram for **1**, **2a**, **2b**. Presumably active states indicated by solid lines.

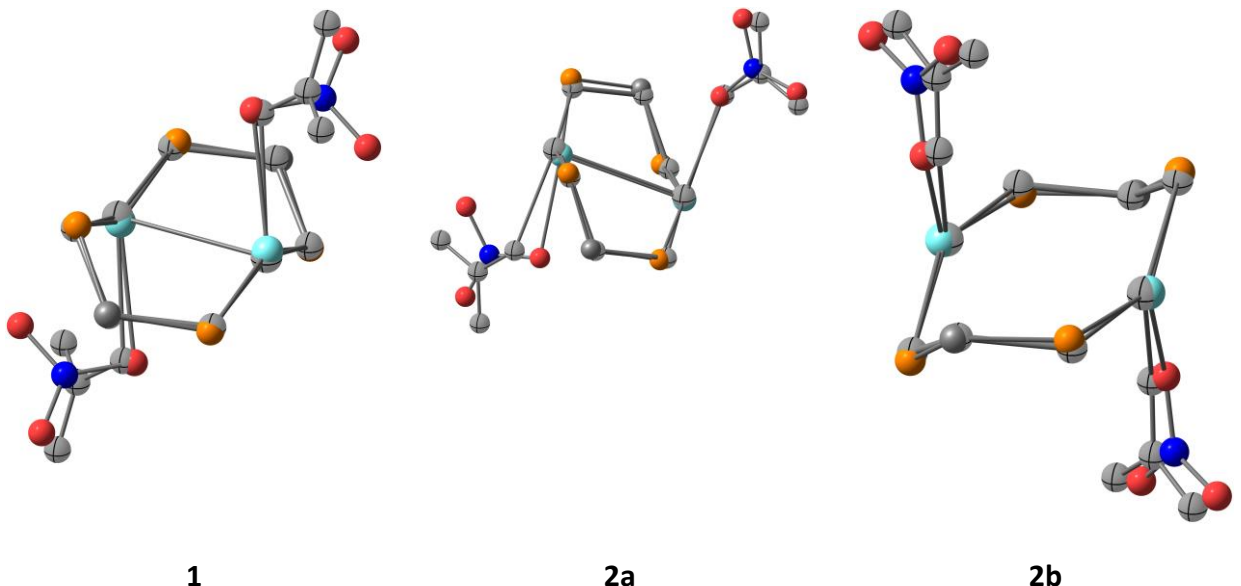


Figure S14. Comparison of X-ray and DFT geometry of $\text{Ag}_2\text{P}_4(\text{NO}_3)_2$ core for **1**, **2a** and **2b**. Atoms of X-ray structure is shaded, DFT structure is colored. Ag – cyan, P – orange, C – gray, O – red, N – blue.

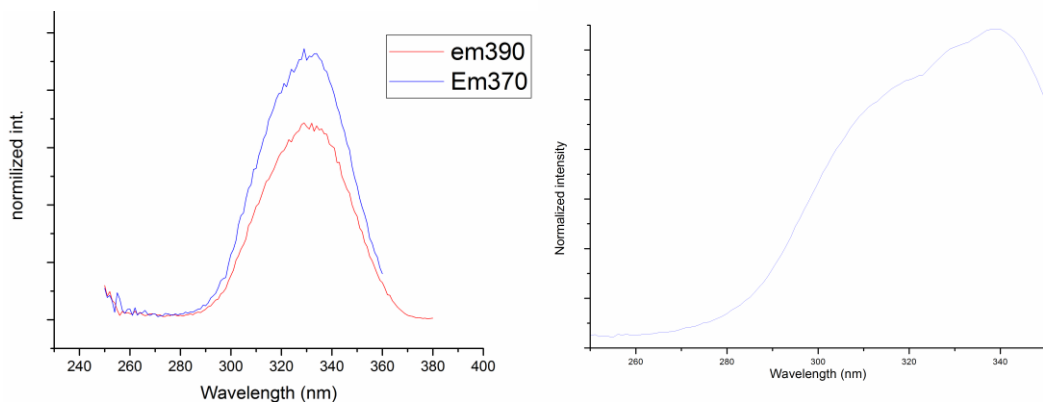


Figure S15. Excitation spectra of **1** in CH_2Cl_2 solution (left, em. on 370 and 390), and in the solid state (right, em. 370)

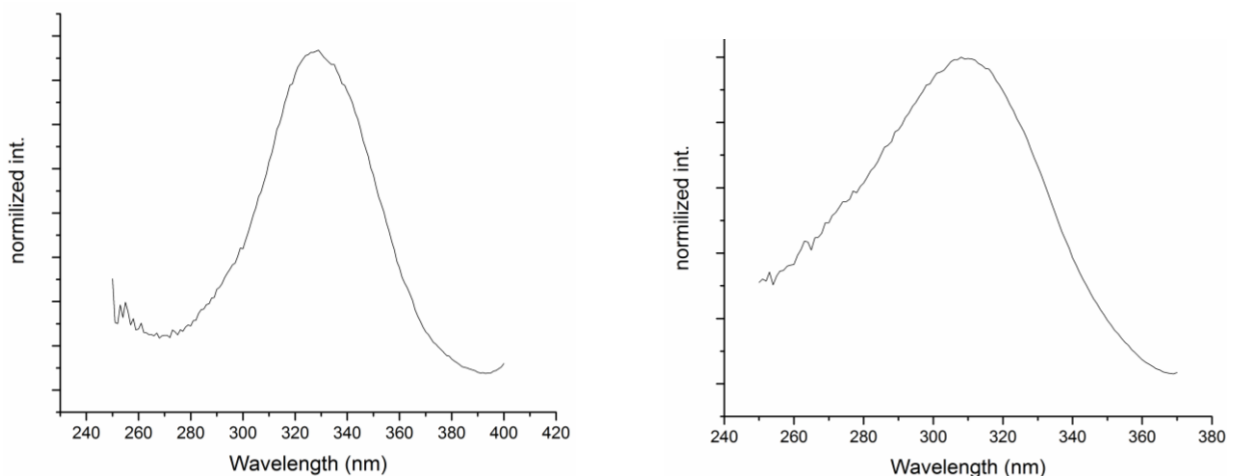


Figure S16. Excitation spectra of **2a** in CH_2Cl_2 solution (left, em. on 410) and in the solid state (right, em. on 380)

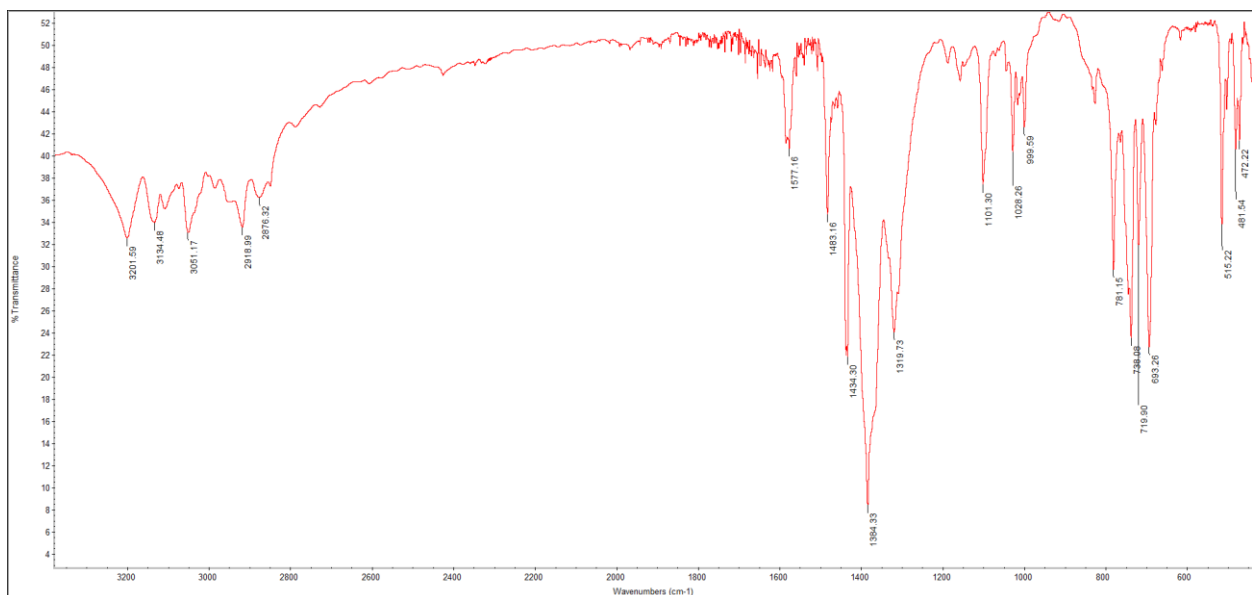


Figure S17. IR spectrum of complex **2a** in KBr pellets.

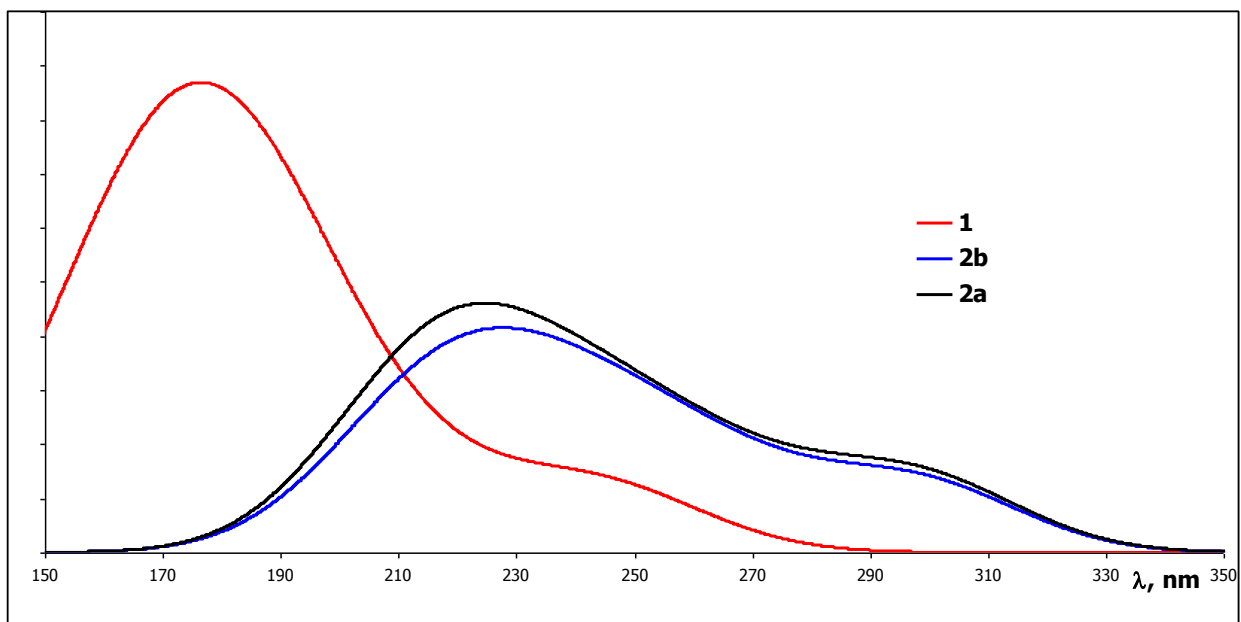


Figure S18. The simulated electronic spectra of **1**, **2a** and **2b**. The 200 lowest energy singlet transitions were considered, and full width at half maximum was set to 40.

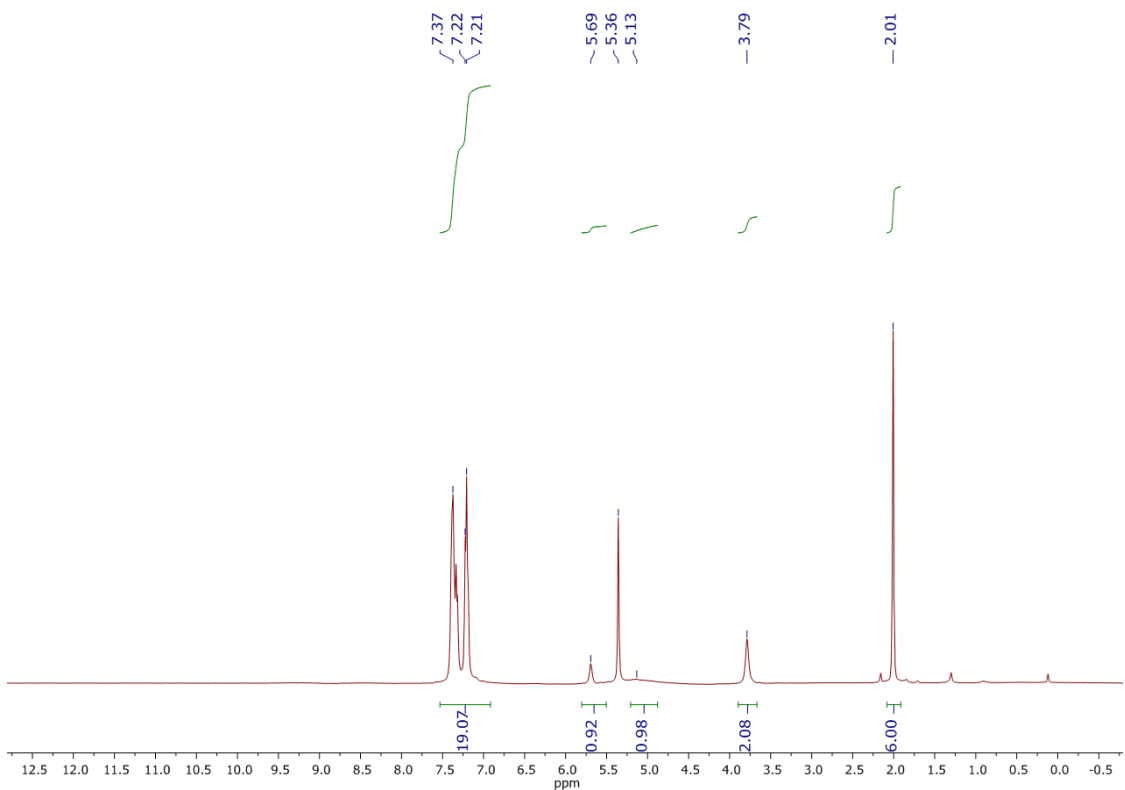


Figure S19. ¹H NMR spectrum of the precipitate obtained in the case of interaction silver nitrate with dppm and Me₂PzH, demonstrating Ag/(Me₂Pz^H)/dppm=1/1/1 ratio, CD₂Cl₂.

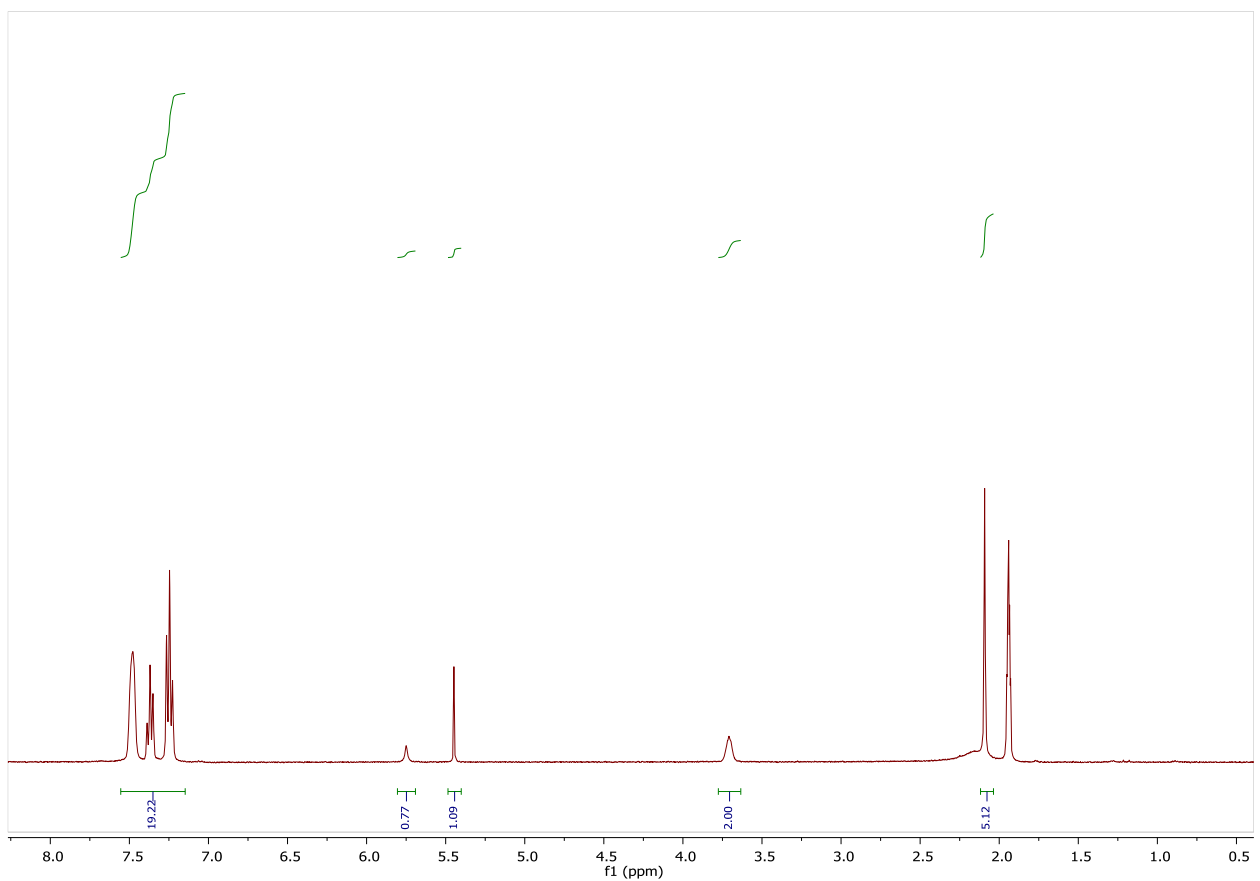


Figure S20. ¹H NMR spectrum of the precipitate obtained in the case of interaction silver nitrate with dppm and Me₂Pz^H, demonstrating Ag/(Me₂Pz^H)/dppm=1/1/1 ratio, CD₃CN.